Spectroscopic method to determine exciton densities, trap interactions, and exciton decay pathways in organic semiconductors

I. Symeonidis [1], V. Podzorov [2] and P. Kounavis [1]
[1]*Department of Electrical and Computer Engineering, University of Patras, 26504 Patras, Greece*
[2]*Department of Physics, Rutgers University, Piscataway, New Jersey 08854, USA*

(Received 17 September 2025; accepted 30 March 2026; published 17 April 2026)

The unique optoelectronic properties of organic semiconductors make them attractive candidates for functional electronic devices. Organic molecules exhibiting singlet fission—a process in which a photoexcited singlet exciton converts into two triplet excitons—hold particular promise for enhancing the efficiency of organic optoelectronic devices. Once generated, triplet excitons decay either through triplet-triplet annihilation (TTA) or interaction with trap states. Identifying these decay pathways is essential for understanding and controlling the performance of organic semiconductors. Modulated photocurrent (MPC) spectroscopy is a useful technique for extracting information about various parameters of the trap states of inorganic and organic semiconductors. Recently, it was shown that in organic semiconductors the MPC is highly sensitive to exciton-trap interactions, where excitons dissociate into mobile holes. Here, using this approach, we present a new spectroscopic method based on MPC for extracting both the triplet exciton density and the density of traps involved in their dissociation in two-terminal organic devices: rubrene single crystals and pentacene thin films. Furthermore, we show that the characteristic dependence of triplet exciton density on the light generation rate enables the separation of different decay pathways. Our results reveal that triplet exciton decay is dominated by TTA in rubrene crystals, while in pentacene films it primarily proceeds via triplet-trap interactions.

DOI: 10.1103/4h9n-cmgt

I. INTRODUCTION

Singlet fission (SF) [1] has attracted significant attention as a strategy to overcome fundamental efficiency limits in organic electronic devices. SF is a fast and efficient multiexciton process in which photoexcited singlet excitons split into pairs of strongly correlated triplet excitons. This mechanism allows the generation of more than one electron-hole pair from a single absorbed photon, making SF highly attractive for optoelectronic applications such as photodetectors [2] and solar cells [3]. Characteristic examples of molecules undergoing SF are pentacene films and rubrene crystals, which are studied in this work. Specifically, SF in pentacene is exothermic and most triplets are generated very rapidly and efficiently by SF [4]. Triplet exciton formation by intersystem crossing (ISC) is relatively very slow and very unlike, whereas the formation of excimers or doubly excited excitons has been ruled out in pentacene films [5]. In rubrene, SF is only slightly endothermic. This allows for the efficient production of triplets from SF [6], while triplet-triplet annihilation (TTA), known as the triplet fusion process, can also occur with high efficiency [7]. ISC is generally considered negligible in rubrene crystals under normal conditions [6].

The generation and decay of triplet excitons, produced by SF [8], can be described by the following rate equation:

$$\frac{dT}{dt} = 2G_b - \gamma_D T D^{tot+} - \gamma_T T^2 = 0. \quad (1)$$

Here, the first term corresponds to the triplet generation rate $G_{SF} = 2G_b$, where the factor of 2 accounts for the formation of two triplets per absorbed photon. Once formed, triplet excitons diffuse and may undergo bimolecular annihilation with a rate $G_{an} = \gamma_T T^2$, where γ_T is the TTA constant [7,9] and T is the triplet exciton density. This process is represented by the third term in Eq. (1).

The second term of Eq. (1) describes the dissociation of triplet excitons into mobile holes via interaction with deep donor-like traps D^+ at a total density of D^{tot+}, which are already present in the dark equilibrium state of the samples and are not photogenerated. These charged traps are donor-like traps, which are not occupied by electrons near or below the dark Fermi level or the quasi-Fermi level of trapped holes, E_{tp}^D, forming a reservoir of positively charged centers, as schematically illustrated in Figs. 1(c) and 1(d) (red regions). The density of D^+ is given by the product of the occupation function of holes and the density of states of donor-like traps. This charge is essentially balanced for the respective negative charge density in the occupied acceptor-like traps, thereby maintaining electrical neutrality, as is described in Appendix B. The D^{tot+} density is maximum in the dark state and, as is shown below, decreases under illumination, due to interaction of triplets with D^+ centers. The dissociation pathway of triplets via D^+ traps—identified by modulated photocurrent (MPC) spectroscopy—was previously established as the key photogeneration mechanism in both pentacene films and rubrene crystals [10]. During diffusion, triplet excitons encounter D^+ centers and undergo an Auger-like process [11] known as triplet-donor–like trap annihilation (TDA) depicted schematically in Figs. 1(c) and 1(d). In this process, the electron from a triplet is captured by a

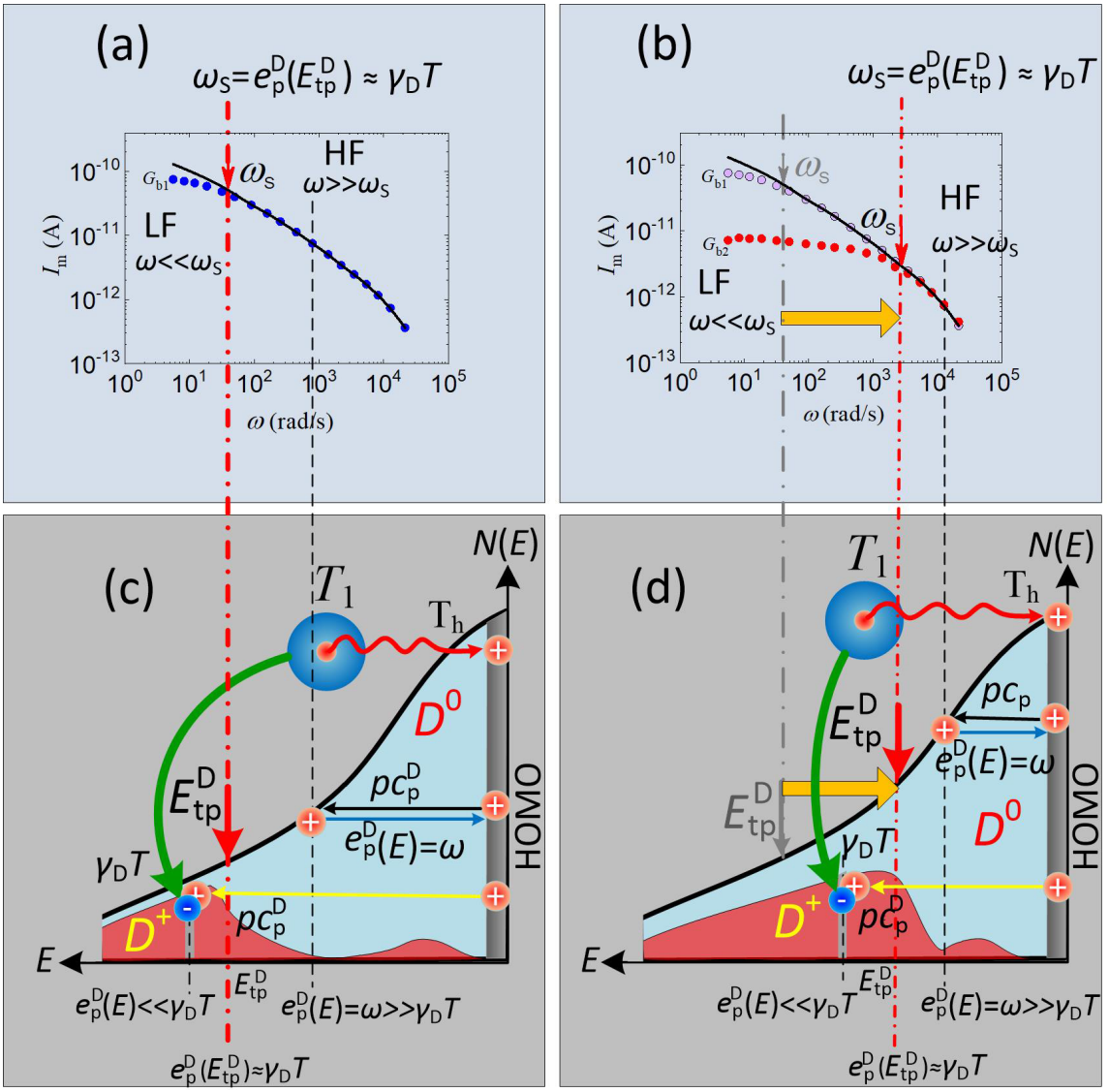

FIG. 1. MPC amplitude spectra and the schematic illustration of hole-trap and triplet-trap interactions contributing to the MPC response. (a), (b) MPC amplitude I_m of rubrene at weak G_{b1} and moderate G_{b2} excitation. (c), (d) Donor-like trap distribution on the HOMO side. Holes interact with neutral traps D^0 via trapping/release, while triplets undergo Auger-like dissociation at D^+ traps, releasing mobile holes. The crossover frequency ω_s corresponds to the quasi-Fermi level E_{tp}^D of trapped holes that shift to higher frequencies and shallower energies, respectively, with increasing G_b.

D^+ center (green arrows $\gamma_D T$) at a total rate $G_{dis} = \gamma_D T D^{tot+}$, where γ_D is the capture probability. The released energy is transferred to the hole, which becomes mobile (wavy arrows T_h) and contributes to the photocurrent until eventually captured by a neutral trap D^0 and recombines (yellow arrows pc_p^D).

MPC is a powerful spectroscopic method for studying the interaction of mobile charge carriers with trap states. Based on this property, it has been applied to extract information about the trapping parameters of inorganic [12–14] and organic semiconductors [15–17]. In organic semiconductors, it has been recently found that the interactions of triplet excitons with donor-like traps affect the dynamics of the corresponding interactions of mobile holes with these donor-like traps captured by the MPC [10]. It was proposed that the MPC can be very useful for providing quantitative insights into both the density of triplet excitons and their dominant decay pathways [10]. This new potential application of the MPC spectroscopy is demonstrated in this work using two-terminal devices based on rubrene single crystals and pentacene films. Specifically, we propose a new spectroscopic method based on the MPC that disentangles the main exciton decay pathways while simultaneously determining the triplet exciton density T, trap density D^{tot+}, and the capture constant γ_D.

II. BACKGROUND OF MPC SPECTROSCOPY

In modulated photocurrent (MPC) spectroscopy, a constant-intensity light beam generates steady-state densities of holes p and triplet excitons T. A weak, sinusoidally modulated probe beam produces an MPC signal with

amplitude I_m, which is recorded as a function of angular modulation frequency ω.

Representative MPC spectra of rubrene crystals under moderate and higher bias light generation rates (G_b) are shown in Figs. 1(a) and 1(b). Similar spectra are obtained for pentacene films. A key parameter of this method is the *crossover frequency* ω_s (red arrows), which divides the MPC spectrum into two distinct frequency regimes [10]. In the *high-frequency (HF) regime* ($\omega \gg \omega_s$), I_m is nearly independent of G_b and spectra for different G_b values overlap, forming an upper envelope (thick solid line). In this regime, MPC originates primarily from interactions between mobile holes and neutral donor-like traps D^0, located shallower than the quasi-Fermi level of trapped holes, E_{tp}^D [10]. These traps are indicated in Figs. 1(c) and 1(d) (blue region).

Mobile holes may be transported either through localized states by hopping or extended states near the top of the highest occupied molecular orbital (HOMO), as depicted in Figs. 1(c) and 1(d) (gray regions). From these states, they interact via trapping-detrapping processes with neutral traps D^0, with capture rate pc_p^D (black arrows) and thermal emission rate $e_p^D(E)$ (green arrows), where c_p^D is the capture coefficient. In the HF regime, the modulation frequencies ω match the thermal emission rates of holes from D^+ traps (dashed lines), i.e., $\omega \cong e_p^D(E) \gg pc_p^D + \gamma_D T$, independent of G_b.

At frequencies around the *crossover point* $\omega \approx \omega_s$, the MPC spectrum transitions to lower values. The crossover frequency corresponds to the emission rate of traps located at the quasi-Fermi level (thick red arrows):

$$\omega_s \approx e_p^D\left(E_{tp}^D\right) \cong pc_p^D + \gamma_D T. \tag{2}$$

Traps deeper than E_{tp}^D have negligible emission rates and are positively charged D^+ forming the reservoir of trapped holes (red regions in Fig. 1). In the *low-frequency (LF) regime* ($\omega \ll \omega_s$), MPC reflects interactions of holes and excitons with these deeper traps. Increasing G_b shifts E_{tp}^D to shallower energies and ω_s to higher frequencies, owing to the increase in p and T.

When the hole contribution becomes negligible ($pc_p^D \ll \gamma_D T$), Eq. (2) reduces to

$$\omega_s \approx \gamma_D T. \tag{3}$$

Equation (3) forms the basis of our method, enabling the extraction of the triplet density from

$$T \cong \frac{\omega_s}{\gamma_D}, \tag{4}$$

by means of the crossover point ω_s of the MPC spectra.

The dependence of ω_s on G_b reveals the dominant exciton decay pathway. If triplet dissociation dominates $\gamma_D D^{tot+} \gg \gamma_T T$,

$$G_{dis} = \gamma_D T D^{tot+} \approx \omega_s D^{tot+} \approx 2G_b, \tag{5}$$

leading to the linear relation

$$\omega_s = \frac{2G_b}{D^{tot+}}. \tag{6}$$

The trap density can thus be estimated as

$$D^{tot+} = \frac{2G_b}{\omega_s}. \tag{7}$$

The light-created triplet density can be determined from Eq. (4) by introducing the constant γ_D, which can be obtained from the literature or by solving Eq. (5) to obtain

$$\gamma_D \approx \frac{2G_b}{TD^{tot+}} = \frac{1}{\tau\, D^{tot+}}, \tag{8}$$

where $\tau = \frac{T}{2G_b}$ is the monomolecular lifetime of triplets, which can be available from other experiments.

Alternatively, if triplet-triplet annihilation dominates ($\gamma_D D^{tot+} \ll \gamma_T T$),

$$G_{an} = \gamma_T T^2 \approx \gamma_T \left(\frac{\omega_s}{\gamma_D}\right)^2 \approx 2G_b, \tag{9}$$

which yields the square-root relation

$$\omega_s \approx \gamma_D (2G_b/\gamma_T)^{1/2}. \tag{10}$$

In this case, γ_D can be estimated as

$$\gamma_D \approx \omega_s/(2G_b/\gamma_T)^{1/2}. \tag{11}$$

III. MATERIALS AND METHODS

A. Sample preparation

Rubrene single crystals with typical (*a*,*b*) facet dimensions of 1–3 mm and thickness ~1 mm were grown by physical vapor transport following the previously published procedure [18]. Crystals with well-defined facets were mounted on substrates with rubber cement and contacted using colloidal graphite paint, which provided reliable electrical contact after drying. Gold wires (25 μm thick) were used for electrical connections. Pentacene films (~250 nm) were deposited on 7059 corning glass substrates by thermal evaporation according to the procedure described elsewhere [19]. Coplanar gold electrodes (0.45 mm spacing, 8 mm length) were evaporated onto the film surface. All devices were mounted in a vacuum optical cryostat and measured at room temperature.

B. MPC measurements

In the MPC spectroscopy, two light-emitting diodes (LEDs) are employed that uniformly illuminate the whole channel area of the samples [20]. In pentacene, both LEDs emitted red light (630 nm), corresponding to singlet absorption and the high-energy Davydov component [19]. In rubrene, both LEDs emitted blue light (460 nm), near the main absorption peak [20]. The LEDs were supplied by RS and their wavelength of maximum output power was measured using a monochromator (Cornerstone-Oriel). One LED served as a sinusoidally modulated probe, while the other provided a stronger constant-intensity bias beam. The red-light illumination provides light absorption throughout the whole film thickness of pentacene films. The blue light illumination is absorbed by rubrene, within the light penetration depth, which is on the order of 5 μm, as estimated from the inverse absorption coefficient of crystalline rubrene. This penetration depth is much smaller than the typical thickness of the crystals and much lower than the distance between the contacts (~mm). Thus all the layers of the crystal at different depths below the surface, in which photoexcitation is distributed following a Beer-Lampert exponent, are essentially connected to the contacts in parallel [21]. In such a "coplanar" geometry,

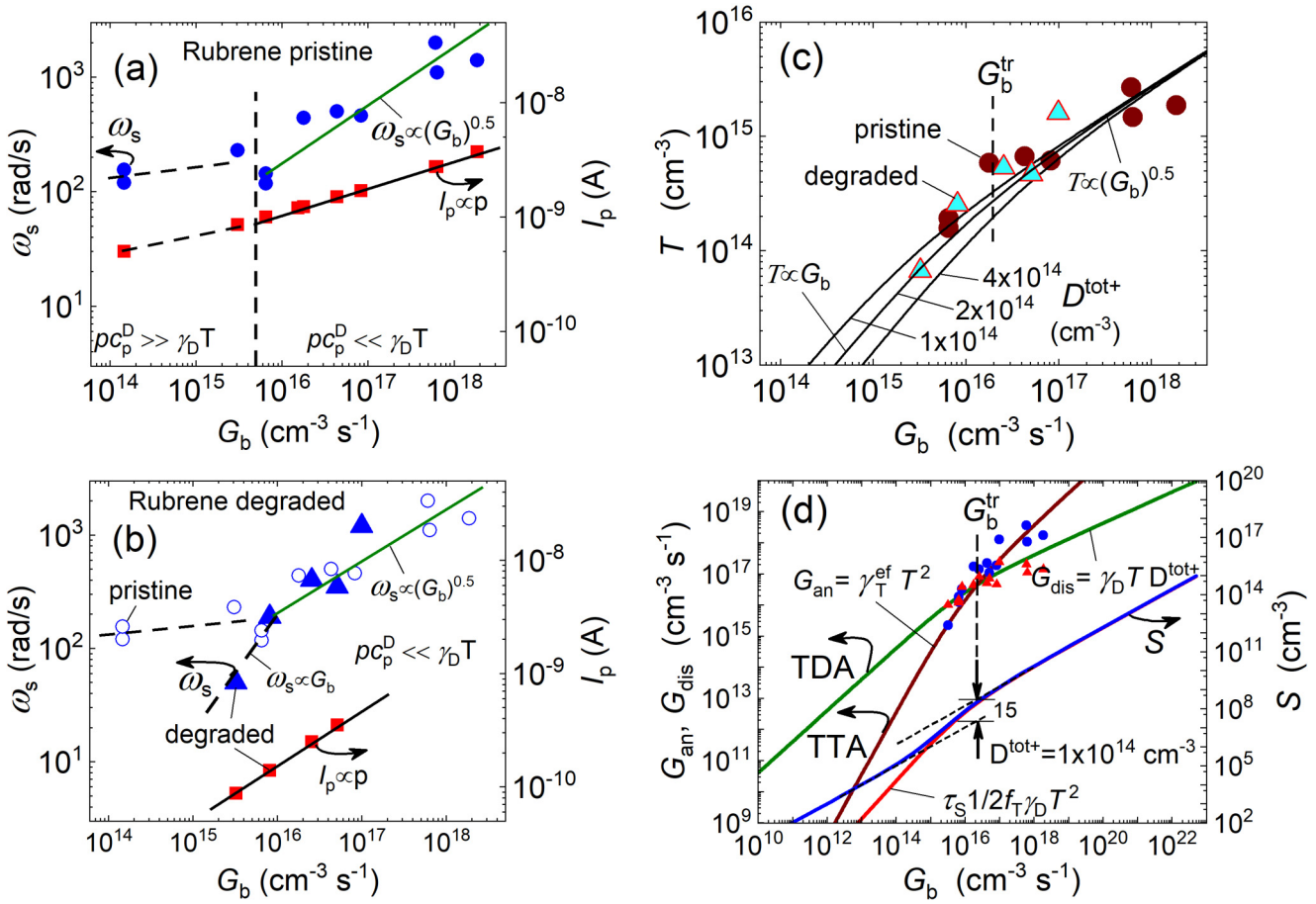

FIG. 2. Dependence of key parameters on the light generation rateG_b in rubrene crystals. (a), (b) Crossover frequency ω_s compared with the dc photocurrent I_p (red solid squares) for pristine and degraded state, respectively. (c) Triplet density T extracted from ω_s (symbols), compared to that calculated from Eq. (A6) (lines) using the indicated trap densities D^{tot+}. (d) Comparison of annihilation $G_{an} = \gamma_T^{ef} T^2$ and dissociation $G_{dis} = \gamma_D T D^{tot+}$ rates, showing transition from TDA to TTA at low transition rate G_b^{tr}, where the singlet exciton density S calculated from Eq. (A9) predicts a characteristic enhancement by a factor of 15.

the voltage applied to each layer is the same (so is the electric field), regardless of the depth, photoexcitation level, or conductivity of individual layers, meaning that no redistribution of the in-plane electric field should occur when the sample is illuminated [21].

Between the two coplanar electrodes of all samples, a small voltage in the range of 1–5 V was applied, which provides ohmic current-voltage characteristics and uniform electric field distribution. In this way, space-charge-limited currents are absent. The dc photocurrent flowing through the samples was measured with a Keithley 6517B electrometer. The MPC photocurrent signal was amplified and detected with a lock-in amplifier (Stanford Research Systems SR830). A silicon PIN photodiode (BPX 65) was used to feed the lock-in amplifier with the reference signal. The MPC amplitude was recorded as a function of modulation frequency ω at different fixed bias-light intensities, measured by a calibrated silicon diode (Newport 918D-UV-OD3).

IV. EXPERIMENTAL RESULTS AND DISCUSSIONS

A. Rubrene single crystals

Figures 2(a) and 2(b) present the crossover frequency ω_s and steady-state photocurrent I_p versus G_b for pristine and degraded rubrene crystals, respectively. In the pristine state, for $G_b \leqslant 5 \times 10^{15}$ cm^{-3}, ω_s closely follows I_p, consistent with the fact that $\gamma_D T$ is negligible in Eq. (2), which then reduces to $\omega_s \approx pc_p^D$. At higher G_b, ω_s rises more steeply than I_p, indicating that in Eq. (2) the term pc_p^D is negligible and that the $\gamma_D T$ contribution dominates, leading to $\omega_s \cong \gamma_D T$ [Eq. (3)]. As shown in Fig. 2(a), ω_s shows a square root dependence $\omega_s \propto (G_b)^{1/2}$. According to Eq. (3), this scaling directly implies also a similar square root dependence $T \propto (G_b)^{1/2}$, confirming that TTA is the primary decay pathway in these pristine crystals. In the pristine state, it is known that only a thin layer on the crystal's surface is primarily responsible for the photogeneration of charge carriers and their transport, whereas the bulk contributions are negligible [20,21]. Nevertheless, the bulk properties of the crystals can also be studied by intentionally deteriorating the electronic properties of the surface layer. This is achieved by exposing the crystal to an operating ion gauge under high-vacuum conditions and manually turning the gauge on and off (for more details see Refs. [20,21]). Here, we use this gauge effect to deliberately induce surface traps, so that the surface layer ceases to contribute to the photocurrent [20]. The photocarrier transport is now governed almost entirely by the bulk of the crystal,

TABLE I. Extracted parameters related to the triplet exciton decay in rubrene and pentacene.

Materials	γ_T (cm^3s^{-1})	γ_D (cm^3s^{-1})	D^{tot+} (cm^{-3})	T (cm^{-3})	Exciton decay pathway
Rubrene crystals	5×10^{-12} [7]	8.0×10^{-13}	$\leqslant 10^{14}$	10^{14}–10^{15}	TTA
Pentacene films	2×10^{-11} [9]	4.8×10^{-7}	$\sim 10^{15}$	10^{8}–10^{10}	TDA

which is not affected by the gauge effect. We have studied rubrene crystals in the degraded state obtained by the gauge effect and the results are presented in Fig. 2(b). In this figure, the ω_s of the degraded state shows a stronger dependence on G_b than that of the photocurrent I_p, indicating that pc_p^D is negligible in Eq. (2), in line with the fact that I_p is reduced by an order of magnitude [20,21], leading to $\omega_s \cong \gamma_D T$. Again, ω_s shows a dependence near that of the square root, indicating that TTA dominates in pristine as well as in degraded crystals, confirming that this annihilation path dominates in the surface layer and in the bulk of the crystals.

The above conclusion aligns with prior studies reporting that rubrene exhibits highly efficient singlet fission and fusion with high equal probabilities f_S and f_T ($f_S \approx f_T \approx 0.95$), respectively, due to energetic resonance between two triplets and one singlet [7,22]. A more quantitative analysis (Appendix A), which incorporates fusion in the rate equations, yields an effective annihilation constant of $\gamma_T^{ef} = (1 - f_S f_T)\gamma_T = 5 \times 10^{-13}$ cm^3. This value replaces γ_T in Eq. (11) from which we estimate $\gamma_D \approx 7.5 \times 10^{-13}$ cm^3s^{-1}. Subsequently, from Eq. (4) we extract the triplet density [Fig. 2(c)], which varies from 10^{14} cm^{-3} to 10^{15} cm^{-3}. These values correspond to average triplet separations (100–200 nm)—well below the diffusion length (∼μm) [23]—further confirming efficient TTA.

Calculations constrain the trap density to an upper bound of $D^{tot+} = 1$–2×10^{14} cm^{-3}. As shown in Fig. 2(c), from the triplet density (solid lines) obtained by solving Eq. (A6), only that calculated using the above upper bound agrees with the experimental values (symbols). Consequently, the transition from the linear to the square root dependence, where the annihilation rate $G_{an} = \gamma_T T^2$ (brown line) begins to exceed the dissociation rate $G_{dis} = \gamma_D T D^{tot+}$ (green line), occurs in Fig. 2(d) in the lowest examined region around $G_b^{tr} \approx 2 \times 10^{16}$ $cm^{-3}s^{-1}$ or lower. As a result, in the rest of the examined higher G_b values, we observe the square root dependence $T \propto (G_b)^{1/2}$.

In the transition region, the singlet exciton density S calculated from Eq. (A9) shows a characteristic enhancement by a factor of 15 [arrows in Fig. 2(d)]. This increase originates from the term $\tau_S \frac{1}{2} f_T \gamma_T T^2$ (red line), which describes singlet recreation via triplet fusion. Such a mechanism is predicted to yield a corresponding enhancement in the photoluminescence (PL) intensity due to radiative recombination of the regenerated singlets. Unfortunately, this prediction cannot be verified here, as existing PL measurements in rubrene crystals have been carried out only at much higher excitation G_b rates exceeding 10^{18} $cm^{-3}s^{-1}$ [7,21]. Nonetheless, those studies reported characteristic PL enhancement, though at excitation rates around 10^{20} $cm^{-3}s^{-1}$, corresponding to higher triplet densities of $T \sim 10^{17}$ cm^{-3} [7,21]. Biaggio and Irkhin [7] suggested that such enhancements in high-G_b rate may originate from impurities, which is consistent with our finding that the onset of triplet fusion in fact occurs at much lower excitation rates.

Overall, the MPC measurements, summarized in Table I, confirm that triplet-triplet annihilation is the dominant decay pathway in rubrene crystals. The respective decay pathway of triplets via interactions with traps, producing mobile holes, occurs as a secondary path under the studied conditions.

B. Pentacene films

Figure 3(a) shows the crossover frequency ω_s and steady-state photocurrent I_p as a function of light generation rate G_b for pentacene films. Here, ω_s increases much more rapidly with G_b than I_p, indicating that the hole term in Eq. (2) is negligible and that the $\gamma_D T$ contribution dominates. Unlike rubrene, here ω_s scales linearly with G_b, i.e., $T \propto G_b$, as predicted by Eq. (6). This linear dependence confirms that triplet dissociation via TDA is the primary decay pathway. The absence of delayed photoluminescence is consistent with this conclusion, since TTA is endothermic in pentacene, where the combined triplet energy lies below that of the singlet.

From Eq. (7), we estimate the trap density as $D^{tot+} \sim 10^{15}$ cm^{-3} [olive triangles in Fig. 3(b)], higher than in rubrene. This difference reflects the greater degree of structural disorder in polycrystalline pentacene films. Using a triplet lifetime of ∼5 ns [24], Eq. (8) yields $\gamma_D \approx 4.8 \times 10^{-7}$ cm^3s^{-1}, consistent with previous reports [25]. The corresponding triplet density spans from 10^8 cm^{-3} to 10^{10} cm^{-3}, which translates into average separations (100 nm–2 μm). These distances are much greater than the triplet diffusion length (40 nm [26]), explaining the inefficiency of TTA under the studied conditions.

Figure 3(b) presents the triplet density T obtained from experimental ω_s data using Eq. (4) (brown circles), alongside values calculated by solving Eq. (1) using the trap density $D^{tot+} \sim 10^{15}$ cm^{-3}. The good agreement between experiment and simulation further validates the extracted parameters. Figure 3(c) compares the annihilation rate $G_{an} = \gamma_T T^2$ and dissociation rate $G_{dis} = \gamma_D T D^{tot+}$ calculated using the respective density T from Fig. 2(b). The results show that G_{an} is negligible compared to G_{dis}, confirming that TDA overwhelmingly dominates exciton decay in pentacene.

Moreover, the calculations predict that a transition from linear to square-root scaling of T [Fig. 2(b)] would only occur at relatively much higher exciton densities, $T > 10^{18}$ cm^{-3}, corresponding to the high-G_b regime. This prediction is consistent with previous transient absorption experiments, which indeed observed bimolecular triplet recombination in that excitation range [9].

Overall, MPC results summarized in Table I demonstrate that, in pentacene films, triplet dissociation via TDA is the dominant decay pathway of triplets, while TTA remains negligible under the present experimental conditions.

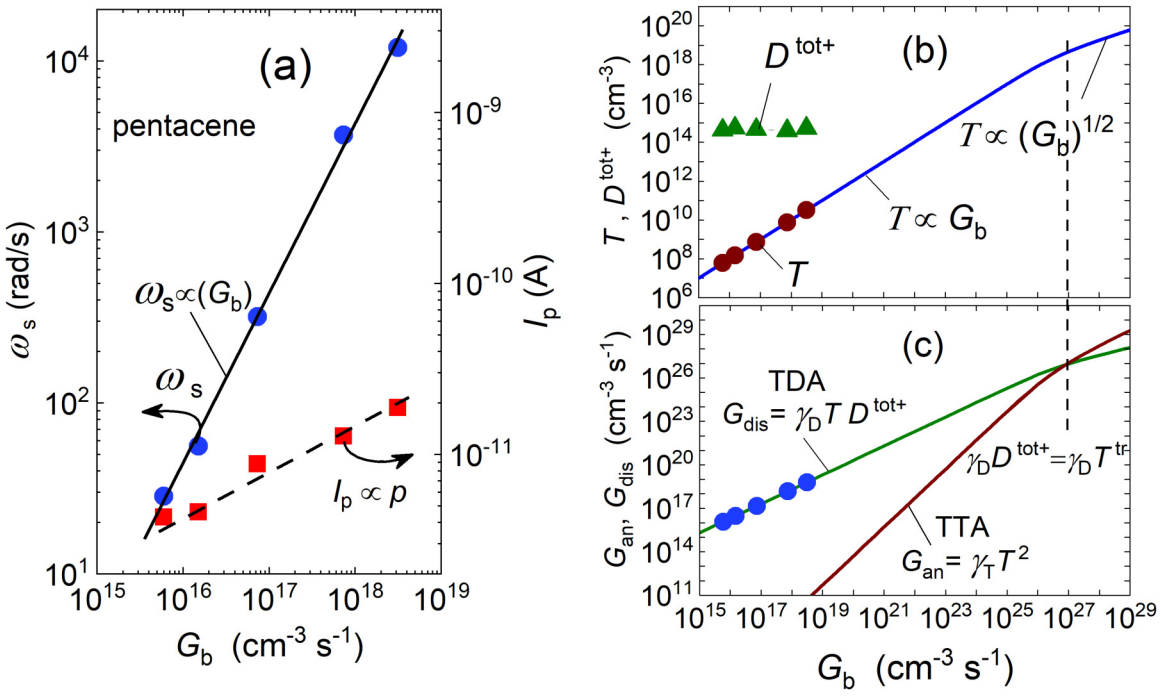

FIG. 3. Dependence of key parameters on the light generation rateG_b in pentacene films. (a) Crossover frequency ω_s (blue circles) compared with the dc photocurrent (red squares). (b) Triplet density T from experiment (brown circles) compared to that from simulations (lines) and trap density D^{tot+} (olive triangles) from experiment. (c) Annihilation $G_{an} = \gamma_T T^2$ and dissociation $G_{dis} = \gamma_D T D^{tot+}$ rates, confirming TDA as the dominant decay pathway.

V. COMPARISON WITH MODEL SIMULATIONS

To validate both the proposed method and the triplet exciton dissociation mechanism, we performed model simulations as described in Appendix B. The results, obtained using the parameters listed in Table I for rubrene, are presented in Fig. 4. The simulations successfully reproduce the experimentally observed transition from linear to square-root scaling of the triplet density T versus G_b at low G_b values [Fig. 4(a)].

The simulations of Fig. 4(b) reveal a power-law dependence for the photoresponse defined by $(p - p_{dark}) \propto (G_b)^a$, with exponents gradually decreasing from 1 to 0.25 and lower as G_b increases. This dependence recovers the respective characteristic power-law photocurrent response $(I_p - I_{dark}) \propto (G_b)^a$, with the same decreasing exponents (inset) [10]. This behavior originates from the progressive depletion of the trapped-hole reservoir due to interactions with triplets. Specifically, the rate $\gamma_D T$ in the denominator of the occupation function [Eq. (B7) Appendix B] increases with G_b, leading to the gradual reduction of D^{tot+} seen in Fig. 4(a). With fewer trapped holes available for triplet dissociation, the photoresponse exponents decrease—an unambiguous signature of the triplet dissociation mechanism via traps. It is worth noting that, in this model, light creates only mobile holes from D^+ centers. No additional electrons are created (see also Appendix B), which is consistent with photo-Hall experiments, from which it was found that electron transport is completely absent [27].

Finally, the results of Fig. 4(d) confirm that $\gamma_D T \gg pc_p^D$, validating the approximation in Eq. (3): $\omega_s \cong \gamma_D T$.

It is important to note that the main conclusions of these simulations do not depend sensitively on the specific parameter choices used in the model.

VI. CONCLUSIONS

We proposed a new method based on the MPC spectroscopy, which proved to be a powerful and versatile tool for studying exciton generation, dissociation, and annihilation in organic semiconductors. This method enables direct determination of both triplet exciton densities and trap densities, while also distinguishing between different decay pathways. We find that, in rubrene crystals, exciton decay proceeds primarily via triplet-triplet annihilation, whereas in pentacene films it is dominated by triplet-trap interactions. The ability to obtain this information from a single experimental technique highlights the utility of MPC spectroscopy in unraveling fundamental processes in organic semiconductors under optical excitation.

ACKNOWLEDGMENTS

V.P. acknowledges support by the Donald H. Jacobs Chair in Applied Physics at Rutgers University (crystal growth). P.K. acknowledges support by the Department of Electrical and Computer Engineering, University of Patras.

DATA AVAILABILITY

The data that support the findings of this article are not publicly available upon publication because it is not

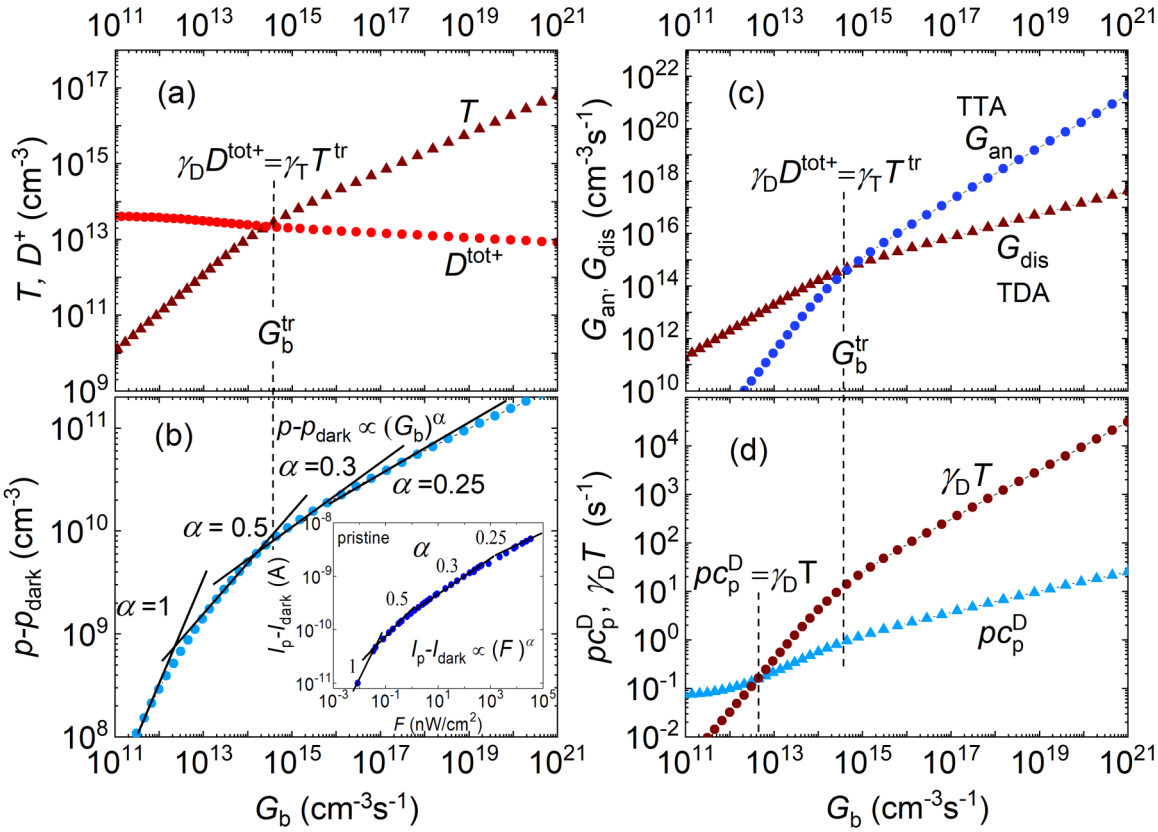

FIG. 4. Representative results of the model simulations reproducing the behavior observed in rubrene crystals. (a) Triplet density T showing the transition from linear to square-root scaling with G_b; trap density D^{tot+} decreases with G_b due to TDA. (b) Power-law dependence $(p - p_{dark}) \propto (G_b)^a$, consistent with experimental photocurrent response (inset). (c) Comparison of dissociation G_{dis} and annihilation G_{an} rates, dominating at low and moderate G_b, respectively. (d) Comparison of rate $\gamma_D T$ with rate pc_p^D, showing that from relatively low G_b values, where $p > p_{dark}$, the condition $\gamma_D T > pc_p^D$ is satisfied, confirming the validity of Eq. (3).

technically feasible and/or the cost of preparing, depositing, and hosting the data would be prohibitive within the terms of this research project. The data are available from the authors upon reasonable request.

APPENDIX A: RATE EQUATIONS OF EXCITONS INCLUDING TRIPLET FUSION

Under steady state light generation rate G_b the rate equation governing the density of the singlet excitons, S, is given by

$$\frac{dS}{dt} = G_b - \frac{S}{\tau_s} = 0, \tag{A1}$$

where τ_s is the lifetime of singlet excitons. Considering that the probability that a singlet exciton undergoes SF is f_S, the generation rate of triplets is $2f_S\frac{S}{\tau_s}$ and the rate equation of triplets of Eq. (1) is written as

$$\frac{dT}{dt} = 2f_S\frac{S}{\tau_s} - \gamma_D T D^+_{all} - \gamma_T T^2 = 0. \tag{A2}$$

In the specific case of rubrene crystals, two colliding triplets recombine to reform singlet excitons with a probability f_T by the fusion process. This is included as an additional term in the rate equation of singlet excitons [Eq. (A1)], which gives

$$\frac{dS}{dt} = G_b - \frac{S}{\tau_s} + \frac{1}{2}f_T\gamma_T T^2 = 0 \tag{A3}$$

from which we take

$$\frac{S}{\tau_s} = G_b + \frac{1}{2}f_T\gamma_T T^2. \tag{A4}$$

Replacing the rate $\frac{S}{\tau_s}$ from Eq. (A4) into Eq. (A2) we take

$$\frac{dT}{dt} = 2f_S G_b + f_S f_T\gamma_T T^2 - \gamma_D T D^+_{all} - \gamma_T T^2 = 0, \tag{A5}$$

which is written as

$$\frac{dT}{dt} = 2f_S G_b - \gamma_D T D^+_{all} - (1 - f_S f_T)\gamma_T T^2 = 0. \tag{A6}$$

Considering that both singlet fission and triplet fusion are taking place very efficiently in rubrene with equal probabilities f_S and f_T very close to unity,

$$f_S \cong f_T \cong 0.95, \tag{A7}$$

it is concluded that Eq. (A6) is essentially Eq. (1) if γ_T is replaced by the effective constant γ_T^{ef} given by

$$\gamma_T^{ef} = (1 - f_S f_T) \cong 1 \times 10^{-1}\gamma_T = 0.1\gamma_T. \tag{A8}$$

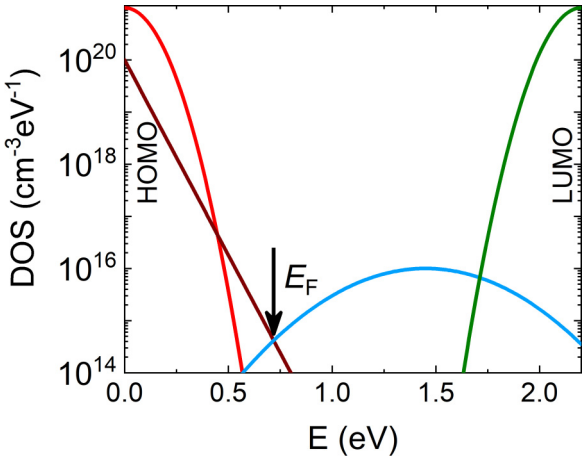

FIG. 5. DOS distribution in the energy gap used in the model simulations. DOS model introduced in the simulations consisting of Gaussian distributions for the HOMO (red line) and LUMO (green line), exponential trap distribution (brown line), and Gaussian deep defect distribution (blue line).

The triplet exciton density can be obtained by solving Eq. (A6), whereas the singlet exciton density can be subsequently calculated from the following relation:

$$S = \tau_s\left(G_\mathrm{b} + \tfrac{1}{2} f_T \gamma_\mathrm{T} T^2\right). \tag{A9}$$

APPENDIX B: MODEL SIMULATION DETAILS

Model calculations were performed assuming the density of states (DOS) distribution of traps in the energy gap, presented in Fig. 5, which is representative of organic semiconductors. Specifically, two Gaussian DOS distributions are assumed for the highest occupied molecular orbital (HOMO) and lowest unoccupied molecular orbital (LUMO), having a typical standard deviation $\sigma = 0.1$ eV and maximum density of $N_{\mathrm{v1}} = N_\mathrm{c} = 1 \times 10^{21}$ cm^{-3} s^{-1}. An exponential tail due to disorder with characteristic slope of $E_\mathrm{o} = 58$ meV and a maximum density of $N_{\mathrm{v2}} = 1 \times 10^{20}$ cm^{-3} s^{-1} is assumed to extend deep in the energy gap above the HOMO. The type of trap states in the side of HOMO are donor-like and have a distribution $D(E)$ given by

$$D(E) = N_{\mathrm{v1}} \exp\left(-\frac{E^2}{2\sigma^2}\right) + N_{\mathrm{v2}} \exp\left(-\frac{E}{E_\mathrm{o}}\right). \tag{B1}$$

A Gaussian distribution $A(E)$ centered at $E_A = 1.45$ eV of deep acceptor-like traps having maximum density $N_\mathrm{A} = 1 \times 10^{16}$ cm^{-3}s^{-1} and standard deviation of $\sigma_A = 0.29$ eV is also assumed:

$$A(E) = N_\mathrm{A} \exp\left(-\frac{(E - E_A)^2}{2{\sigma_A}^2}\right). \tag{B2}$$

The above trap distributions provide that the Fermi level E_F is closer to the HOMO, ensuring that the holes are the majority carriers and reproducing the p-type conduction of the organic semiconductors examined here.

Mobile holes from their transport path can be captured by the D^0 centers at energy E above the transport path with a capture probability $c_\mathrm{p}^\mathrm{D} = 1 \times 10^{-10}$ cm^{-3}s^{-1}. The trapped holes from the resulting D^+ centers are thermally emitted back to the conducting states with a thermal emission rate $e_\mathrm{p}^\mathrm{D}(E)$ given by

$$e_\mathrm{p}^\mathrm{D}(E) = c_\mathrm{p}^\mathrm{D} N_{\mathrm{v1}} \exp\left(-\frac{E}{kT}\right). \tag{B3}$$

Alternatively, mobile holes can be captured by negative acceptor-like trap centers A^- with a capture probability $c_\mathrm{p}^\mathrm{A} = 1 \times 10^{-9}$ cm^{-3}s^{-1}, which is considered ten times higher than the respective c_p^D of the neutral D^0 traps. The trapped holes can be thermally released from the resulting A^0 centers to the conducting states with a thermal emission rate $e_\mathrm{p}^\mathrm{A}(E)$ given by

$$e_\mathrm{p}^\mathrm{A}(E) = c_\mathrm{p}^\mathrm{A} N_\mathrm{v} \exp(-E/kT). \tag{B4}$$

It is worth noting that according to the present model light creation of electrons either by light excitation from the HOMO band or from exciton dissociation is not taking place. Hence the simulated mobile electron density is found negligible, which is supported from the fact that the transport of electrons has been found completely absent [27]. Therefore, the respective electron capture rates of mobile electrons into the traps are negligible [10].

In the steady state condition under illumination, the rates of hole trapping, hole thermal emission, and electron transfer from triplets are in equilibrium and provide that the occupation function of the donor-like traps is given by [10]

$$f^D(E) \cong \frac{e_\mathrm{p}^\mathrm{D}(E) + \gamma_\mathrm{D} T}{p c_\mathrm{p}^\mathrm{D} + e_\mathrm{p}^\mathrm{D}(E) + \gamma_\mathrm{D} T_\mathrm{b}}, \tag{B5}$$

which is a modified occupation function from that of the Shockley-Read-Hall statistics, since it contains the additional electron transfer rate $\gamma_\mathrm{D} T$ from the triplets to the positive traps. Since the acceptor-like traps do not interact with the triplets [7,10], their occupation function is according to the Shockley-Read-Hall statistics and is given by

$$f^\mathrm{A}(E) \cong \frac{e_\mathrm{p}^\mathrm{A}(E)}{p c_\mathrm{p}^\mathrm{A} + e_\mathrm{p}^\mathrm{A}(E)}. \tag{B6}$$

The basis of the model simulations is the charge neutrality condition, which states that the total number of holes (free and trapped) equals the total number of electrons (only trapped, because the free electrons are negligible). The trapped holes are determined by the occupation function of trapped holes given by

$$(1 - f^\mathrm{D}(E)) \cong \frac{p c_\mathrm{p}^\mathrm{D}}{p c_\mathrm{p}^\mathrm{D} + e_\mathrm{p}^\mathrm{D}(E) + \gamma_\mathrm{D} T_\mathrm{b}}. \tag{B7}$$

Note that, in the above expressions of the occupation functions, the contributions from the electrons are omitted, because as mentioned above, these are negligible. In this way, the charge neutrality condition is written as

$$p + \int_{E_\mathrm{v}}^{E_\mathrm{C}} \frac{p c_\mathrm{p}^\mathrm{D}}{p c_\mathrm{p}^\mathrm{D} + e_\mathrm{p}^\mathrm{D}(E) + \gamma_\mathrm{D} T} D(E)\mathrm{d}E \cong \int_{E_\mathrm{v}}^{E_\mathrm{C}} \frac{e_\mathrm{p}^\mathrm{A}(E)}{p c_\mathrm{p}^\mathrm{A} + e_\mathrm{p}^\mathrm{A}(E)} A(E)\mathrm{d}E. \tag{B8}$$

The integrands of the left- and right-hand sides of Eq. (B8) represent the total trapped positive $D^{\text{tot}+}$ density in the donor-like traps and the total trapped negative $A^{\text{tot}-}$ charge density into the acceptor-like traps, respectively. Equation (B8) is used to estimate numerically the hole density p for a given triplet exciton density T created by SF. Subsequently, introducing into Eq. (A6) the derived T and p, the respective G_{b} is calculated. The above process is repeated for different triplet densities T for which the respective hole p and G_{b} are determined. The results of these simulations are plotted as a function of G_{b} in Fig. 4.

[1] M. B. Smith and J. Michl, Recent advances in singlet fission, Annu. Rev. Phys. Chem. **64**, 361 (2013).

[2] H. Ren, J.-De Chen, Y. Q. Li, and J. X. Tang, Recent progress in organic photodetectors and their applications, Adv. Sci. **8**, 2002418 (2021).

[3] M. C. Hanna and A. J. Nozik, Solar conversion efficiency of photovoltaic and photoelectrolysis cells with carrier multiplication absorbers, J. Appl. Phys. **100**, 074510 (2006).

[4] M. B. Wilson, A. Rao, B. Ehrler, and R. H. Friend, Singlet exciton fission in polycrystalline pentacene: From photophysics toward devices, Acc. Chem. Res. **46**, 1330 (2013).

[5] A. Rao, M. W. B. Wilson, S. Albert-Seifried, R. Di Pietro, and R. H. Friend, Photophysics of pentacene thin films: The role of exciton fission and heating effects, Phys. Rev. B **84**, 195411 (2011).

[6] L. Ma, K. Zhang, C. Kloc, H. Sun, M. E. Michel-Beyerlea, and G. G. Gurzadyan, Singlet fission in rubrene single crystal: Direct observation by femtosecond pump–probe spectroscopy, Phys. Chem. Chem. Phys. **14**, 8307 (2012).

[7] I. Biaggio and P. Irkhin, Extremely efficient exciton fission and fusion and its dominant contribution to the photoluminescence yield in rubrene single crystals, Appl. Phys. Lett. **103**, 263301 (2013).

[8] M. Shao, Li Yan, M. Li, I. Ilia, and B. Hu, Triplet–charge annihilation versus triplet–triplet annihilation in organic semiconductors, J. Mater. Chem. C **1**, 1330 (2013).

[9] A. D. Poletayev, J. Clark, M. W. B. Wilson, A. Rao, Y. Makino, S. Hotta, and R. H. Friend, Triplet dynamics in pentacene crystals: Applications to fission-sensitized photovoltaics, Adv. Mater. **26**, 919 (2014).

[10] P. Kounavis and I. Symeonidis, Exciton dissociation mechanism and exciton density in organic semiconductors by modulated-photocurrent spectroscopy, Phys. Rev. Mater. **8**, 113807 (2024).

[11] A. Hangleiter, Nonradiative Recombination via deep impurity levels in semiconductors: The excitonic Auger mechanism, Phys. Rev. B **37**, 2594 (1988).

[12] R. Bruggemann, C. Main, J. Berkin, and S. Reynolds, An evaluation of phase-shift analysis of modulated photocurrents, Philos. Mag. B **62**, 29 (1990).

[13] P. Kounavis, Various defect states in *a*-Si:H studied by modulated photoconductivity spectroscopy, Phys. Rev. B **65**, 155207 (2002).

[14] C. Longeaud, J. A. Schmidt, and R. R. Koropecki, Determination of semiconductor band gap state parameters from photoconductivity measurements. II. Experimental results, Phys. Rev. B **73**, 235317 (2006).

[15] H. Naito, Modulated photocurrent study of localized-state distributions in copper phthalocyanine thin films, J. Appl. Phys. **80**, 5089 (1996).

[16] T. Tanaka, M. Matazuma, and R. Hirohashi, Modulated photocurrent of evaporated copper phthalocyanine thin films, Thin. Solid. Films **322**, 290 (1998).

[17] S. Gorgolis, A. Giannopoulou, and P. Kounavis, Charge carriers' trapping states in pentacene films studied by modulated photocurrent, J. Appl. Phys. **113**, 123102 (2013).

[18] R. W. I. de Boer, M. E. Gershenson, A. F. Morpurgo, and V. Podzorov, Organic single-crystal field-effect transistors, Phys. Status Solidi A **201**, 1302 (2004).

[19] S. Gorgolis, A. Giannopoulou, D. Anastassopoulos, and P. Kounavis, Impact of pentacene film thickness on the photoresponse spectra: Determination of the photocarrier generation mechanism, J. Appl. Phys. **112**, 013101 (2012).

[20] N. Vagenas, V. Podzorov, and P. Kounavis, Modulated-photocurrent spectroscopy of single-crystal organic semiconductor rubrene with pristine and trap-dominated surfaces, Phys. Rev. Mater. **5**, 063801 (2021).

[21] P. Irkhin, H. Najafov, and V. Podzorov, Steady-state photoconductivity and multi-particle interactions in high-mobility organic semiconductors, Sci. Rep. **5**, 15323 (2015).

[22] A. Ryasnyanskiy and I. Biaggio, Triplet exciton dynamics in rubrene single crystals, Phys. Rev. B **84**, 193203 (2011).

[23] H. Najafov, B. Lee, Q. Zhou, L. C. Feldman, and V. Podzorov, Observation of long-range exciton diffusion in highly ordered organic semiconductors, Nat. Mater. **9**, 938 (2010).

[24] A. Rao, M. W. B. Wilson, J. M. Hodgkiss, S. Albert-Seifried, H. Bässler, and R. H. Friend, Exciton fission and charge generation via triplet excitons in pentacene/C_{60} bilayers, J. Am. Chem. Soc. **132**, 12698 (2010).

[25] M. Tabachnyk, B. Ehrler, S. Bayliss, R. H. Friend, and N. C. Greenham, Triplet diffusion in singlet exciton fission sensitized pentacene solar cells, Appl. Phys. Lett. **103**, 153302 (2013).

[26] N. A. Pace, N. V. Korovina, T. T. Clikeman, S. Holliday, D. B. Granger, G. M. Carroll, S. U. Nanayakkara, J. E. Anthony, I. McCulloch, S. H. Strauss, O. V. Boltalina, J. C. Johnson, G. Rumbles, and O. G. Reid, Slow charge transfer from pentacene triplet states at the Marcus optimum, Nat. Chem. **12**, 63 (2020).

[27] V. Bruevich, H. Ho Choi, and V. Podzorov, The photo-Hall effect in high-mobility organic-semiconductors, Adv. Funct. Mater. **31**, 2006178 (2021).